

**Origin of the extra low creep
ductility of copper without
phosphorus**

Rolf Sandström, Corrosion and Metals Research Institute
Materials Science and Engineering, KTH

Rui Wu, Corrosion and Metals Research Institute

February 2007

Svensk Kärnbränslehantering AB

Swedish Nuclear Fuel
and Waste Management Co
Box 5864

SE-102 40 Stockholm Sweden

Tel 08-459 84 00
+46 8 459 84 00

Fax 08-661 57 19
+46 8 661 57 19



Origin of the extra low creep ductility of copper without phosphorus

Rolf Sandström, Corrosion and Metals Research Institute
Materials Science and Engineering, KTH

Rui Wu, Corrosion and Metals Research Institute

February 2007

Keywords: Creep, Ductility, Copper, Phosphorus, Cavitation.

This report concerns a study which was conducted for SKB. The conclusions and viewpoints presented in the report are those of the authors and do not necessarily coincide with those of the client.

A pdf version of this document can be downloaded from www.skb.se

Abstract

Around 1990 it was discovered that pure copper could have extra low creep ductility in the temperature interval 180 to 250°C. If 50 ppm phosphorus was added to the material the low creep ductility disappeared. A creep cavitation model is presented that can quantitatively describe the observed creep ductility for copper with and without phosphorus. A new model called the double ledge model has been introduced that explains why the nucleation rate of creep cavities is often proportional to the creep rate. The phosphorus agglomerates at the grain boundaries, locks their sliding and thereby reduces the formation and growth of cavities. This is the main reason why extra low creep ductility does not occur in phosphorus alloyed copper.

Contents

1	Introduction	7
2	Reassessment of cavitation in Cu-OF	9
2.1	Previous studies	9
2.2	New metallography	10
3	Nucleation of creep cavities with the double ledge model	15
4	Growth of cavities	17
5	Creep deformation and rupture	19
6	Model predictions	21
6.1	Constants used in the computations	21
6.2	Nucleation and cavity growth	21
6.3	Ductility	24
7	Discussion	27
8	Conclusions	29
	Acknowledgments	29
	References	31

1 Introduction

According to the Swedish KBS-3 concept, spent nuclear fuel will be encapsulated in an inner cylindrical iron container and outer copper canister. The waste package will be deposited 500 m down in granitic bedrock. The canisters will be subjected to temperatures up to 100°C and external stresses up to 15 MPa for several decades /1/. These conditions will cause creep of the copper canisters and the maximum creep deformation is estimated to be as high as 5% /1/. To ensure safe operation, creep properties of the copper must be known. Especially the creep ductility must be adequate to withstand deformations during the initial phase of the storage and possible earthquakes following a glaciation.

Initially it was planned that pure copper Cu-OF would be used for the canisters. However, around 1990 it was discovered that pure copper could have *extra low creep ductility* (ELCD) with elongation values below 1% /2/, /3/. Two of the batches showed these low ductility values but not a third batch, nor did a fourth batch tested later /4/. Light microscopy, scanning electron microscopy (SEM), and Auger were performed for some of the specimens. The metallography is briefly reported in /2/. All studied specimens failed in an intercrystalline way even down to 75°C. Cavitation was found on all the specimens, although to a varying extent even if ELCD was found. Some of cavities were observed around small inclusions, possibly sulphides, which implied that sulphur could embrittle the material. That this represented a real possibility was further supported by the Auger analysis, which demonstrated sulphur content at grain boundaries in the investigated specimens.

The explanation for ELCD given in /2/ may, however, not be a general one. Copper with about 50 ppm phosphorus (Cu-OFP), which is now the main candidate material has been creep tested extensively between 75 and 300°C. The rupture elongation has always been observed to be larger than 14% /4/, /5/. There is no indication of ELCD. Korzhavyi et al. /6/ have proposed a mechanism for a reduced sulphide formation in the presence of phosphorous. However, cavitation and crack formation around sulphides have been observed also for Cu-OFP.

In the present report the metallography of the cavity formation in Cu-OF and to some extent in Cu-OFP is reassessed. The nucleation and growth of the creep cavities are modelled. It is the purpose of the report to explain the observed creep ductility with the aid of the modelled creep cavitation.

2 Reassessment of cavitation in Cu-OF

2.1 Previous studies

A summary of previous creep results is given in Table 2-1, together with the sulphur content. From Table 2-1 it can be seen that some batches of Cu-OF exhibited ELCD. For instance, batch 000 showed ELCD at temperatures higher than 180°C at stresses of 40–100 MPa. Batch 100 also gave ELCD at 215°C at stresses 45–85 MPa. Unfortunately, there are no creep data available at other test conditions.

In addition to batches 000 and 100, one more batch 175_1 of Cu-OF was creep tested at 175°C at stresses of 100–150 MPa /4/, see Table 2-1. The creep elongation varied between 5 and 15%. These values are higher than those for batches 000 and 100. For Cu-OFP, the creep elongations at failure are much higher, namely 14–46% /4/, /5/.

In order to identify the reasons causing ELCD, examinations by means of light optical microscopy, SEM and Auger were carried out in selected creep tested samples having both ELCD and sufficient creep ductility. The results, reported in /2/, /3/, /5/ can be summarised briefly as follows:

1. Creep cavities and cracks are observed to a varying extent on all samples, independent of creep ductility.
2. Creep samples failed intergranularly, independent of creep ductility.
3. ELCD appears fairly independent of time to rupture.
4. Creep cavitation appears around assumed small intergranular inclusions, independent of creep ductility.
5. Auger examinations reveal that the amount of sulphur at fractured grain boundary is 8 at.% for two samples from batch 100, and 2 at.% for one sample from batch 200. The amount of sulphur was 10, 10, and 6 ppm and the grain sizes were 60, 370, and 45 µm in batch 000, 100, and 200, respectively. If all or most of the sulphur out of solution ended up at the grain boundaries, it would have given 0.36, 2.20, 0.09 atom layers at the grain boundaries. Therefore, ELCD was attributed to sulphur embrittlement. No Auger investigations have been reported for batch 000.

Table 2-1. A summary of previous creep results of Cu-OF and Cu-OFP.

Series	S% (ppm)	Grain size	Product form	Creep ductility/ELCD*	Stress (MPa)	Temp. (°C)	Ref.
Batch 000, Cu-OF	10	60	100×100 mm forged bar	ELCD 5–35%	40–100 90–170	180, 215, 250 75–145	/2/, /3/ /7/
Batch 100, Cu-OF	10	370	100×100 mm forged bar**	ELCD	45–85	215	/2/, /3/
Batch 200, Cu-OF	6	45	Ø10 mm bar extruded at 800°C	> 10%	45–100	215	/2/, /3/
Batch 175_1, Cu-OF	6	300	Extruded bar	5–15%	100–150	175	/4/
Batch 500, Cu-OFP	6	115	300×300×25 mm plate	14–46%	40–120	215–350	/5/

* Extra low creep ductility (creep ductility ≤ 1%).

** Material taken from the edge of two 100×100 mm forged bars, which had been electron beam welded together longitudinally.

Even if the sulphur embrittlement could be a reason causing ELCD in copper, some questions still remain:

1. Batch dependence of ELCD. Batch 200 of Cu-OF showed creep ductility greater than 10% at 215°C at stresses of 45–100 MPa. Batch 175_1, which would be prone to ELCD according to previous criteria, did not show any danger of ELCD.
2. Dependence of ELCD on temperature. Batch 000, which showed ELCD at temperatures higher than 180°C, displayed higher creep ductility of 5–35% at lower temperatures than 140°C.
3. Dependence of ELCD on grain size. Coarse grain results in reduced grain boundary area per unit volume. This leads to higher concentration of impurity like sulphur on the grain boundary, if the amount of impurity is constant and if the impurity segregates preferably to the grain boundaries. In fact, ELCD occurs in both fine (batch 000) and coarse grained material (batch 100).
4. Dependence of ELCD on intergranular inclusions. On the one hand, it is common that creep cavitation takes place at the interface between inclusions and matrix, simply because the binding force between inclusions such as sulphides and matrix is weak and the interface opens up easily. This has been demonstrated in previous studies /2/, /3/, /5/. On the other hand, it is an open question of how many sulphides could be formed and if the sulphides could play a major role since the bulk sulphur content in batches 000 and 100 is only 10 ppm.

2.2 New metallography

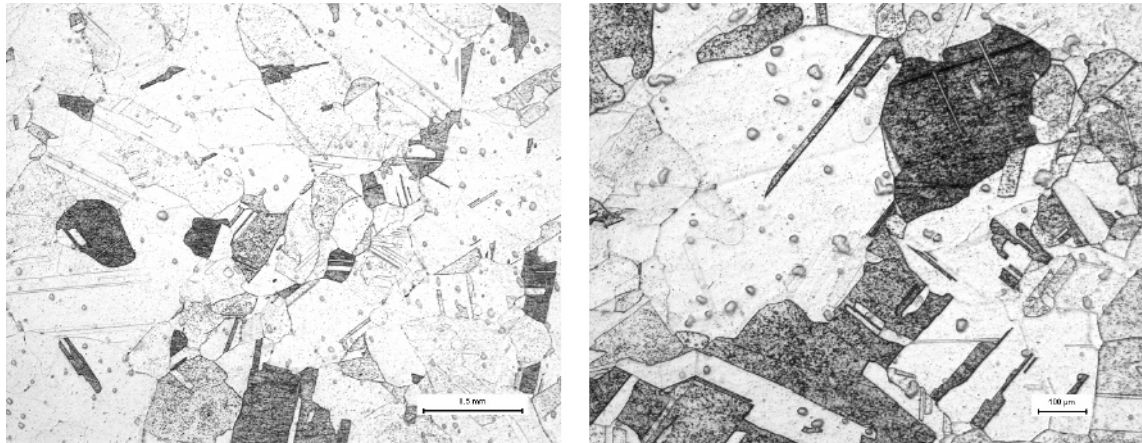
Because of the uncertainties about the amount and role of the sulphide inclusions, a reassessment of the microstructure of the previously tested Cu-OF has been performed. Some representative creep tested samples, see Table 2-2, were selected and examined using light optical microscopy (LOM), analytical scanning electron microscopy (ASEM) and INCA analysis system.

Table 2-2. Current results of microstructural characterisation on selected creep tested samples.

Sample	Series	Chemical composition	T (°C)/ σ (MPa)/ t_R (h)	ϵ_R (%)	Microstructural characterisation	Ref.
Cu14	Batch 000	10 ppm S 2 ppm P 0.16 ppm H 9 ppm Zn	145 / 75 / 5,356	4.9	Mixed grain sizes, twins, intercrystalline failure, creep cracks mainly at fracture, surface crack.	/7/
Cu52	Batch 000	10 ppm S 2 ppm P 0.16 ppm H 9 ppm Zn	250 / 40 / 1,660	0.7	Mixed grain sizes, twins, intercrystalline failure, creep cracks over gauge length, surface crack.	/2/, /3/
Cu15	Batch 000	10 ppm S 2 ppm P 0.16 ppm H 9 ppm Zn	75 / 140 / 6,300	19.5	Mixed grain sizes, twins, intercrystalline failure, creep cracks over gauge length, surface crack.	/7/
Cu51	Batch 000	10 ppm S 2 ppm P 0.16 ppm H 9 ppm Zn	250 /20 / > 16,272	> 0.3	Mixed grain sizes, twins, intercrystalline failure, extensive creep damage over gauge length, surface crack.	/2/, /3/
Cu101	Batch 100	10 ppm S 2 ppm P 0.69 ppm H < 1 ppm Zn	215 / 45 / 684	0.6	Mixed grain sizes, twins, intercrystalline failure, creep cracks over gauge length, surface crack.	/2/, /3/
Cu204	Batch 200	6 ppm S < 1 ppm P < 0.1 ppm H < 1ppm Zn	215 / 85 / 1,030	11.1	Uniform grain sizes, twins, intercrystalline failure, creep cracks over gauge length, surface crack.	/2/, /3/

T , σ , t_R and ϵ_R refer to temperature in °C, stress in MPa, time to rupture in hour and creep strain at rupture in %, respectively.

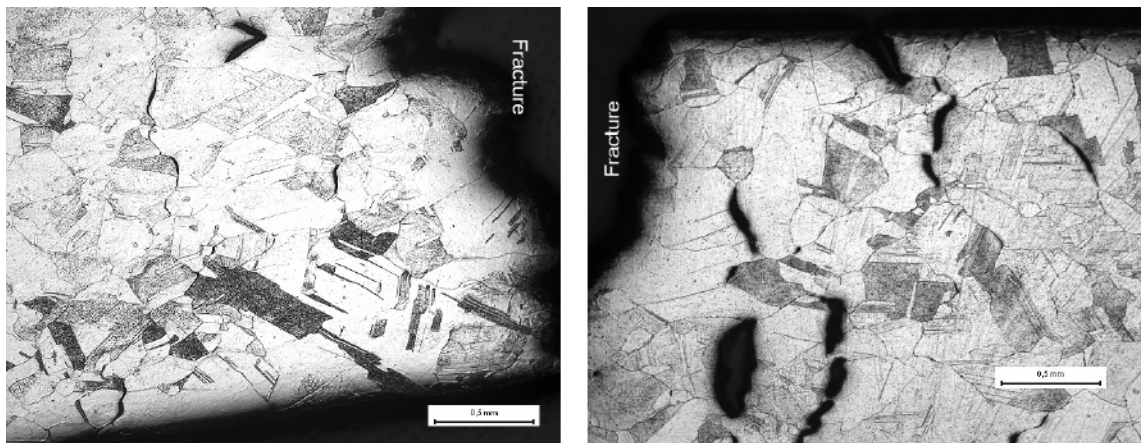
Samples used for microscopic examinations were metallographically prepared and etched in a solution containing 40 g CrO₃, 7.5 g HN₄Cl, 50 ml H₂SO₄, 50 ml HNO₃ and 1,900 ml H₂O. As previously observed all the batches of Cu-OF showed twins and mixed grain sizes, see Figure 2-1 and Table 2-2. Failure took place intergranularly, obviously insensitive to creep test conditions and ductility, see Figure 2-2.



(a) Cu51

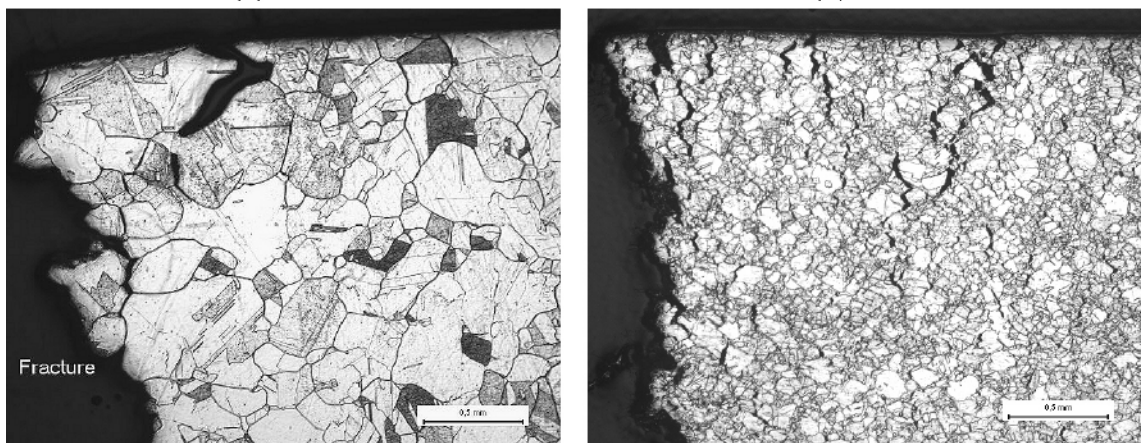
(b) Cu15

Figure 2-1. LOM images showing twins and mixed grain sizes. Material data is given in Table 2-2.



(c) Cu15

(d) Cu52



(e) Cu101

(f) Cu 204

Figure 2-2. LOM images showing intergranular fracture. Material data is given in Table 2-2.

Creep damages in the form of grain boundary cavities and cracks are found over the gauge length of creep samples, see Figure 2-3, although there is a trend that extension and amount of creep damage increase with decreasing ductility. These features are in agreement with previous findings. However, current investigations also show surface cracks, see Figure 2-2.

Creep cavitations are in many cases not associated with apparent grain boundary inclusions, see Figure 2-4. Instead, creep cavities and cracks are observed to occur frequently at other positions at grain boundaries.

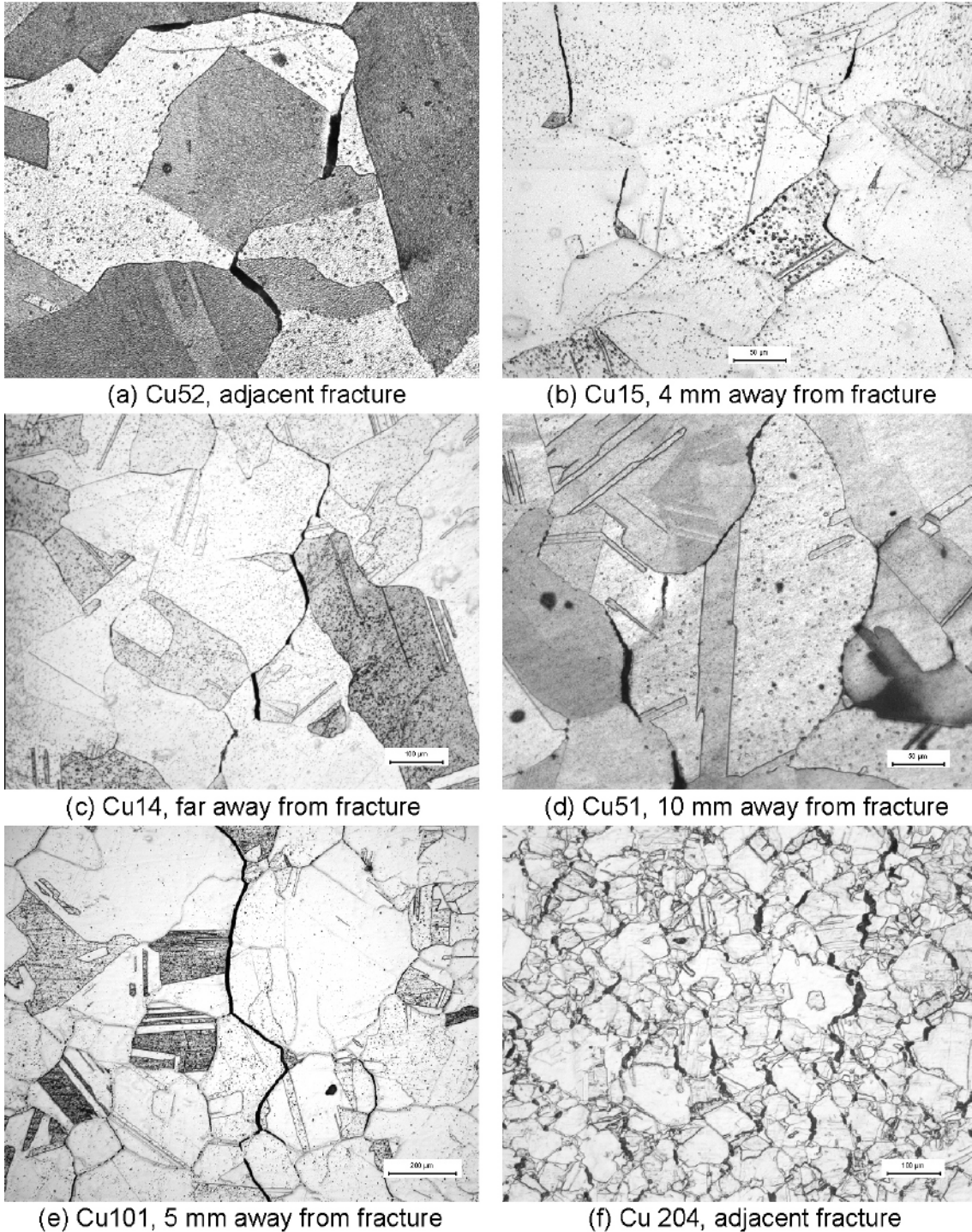
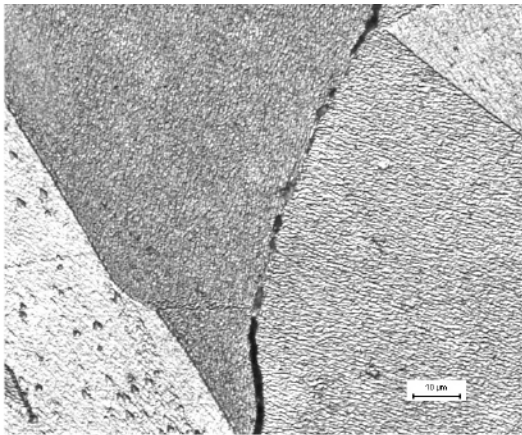
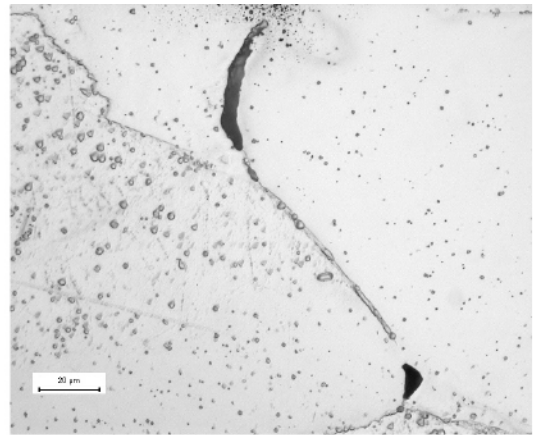


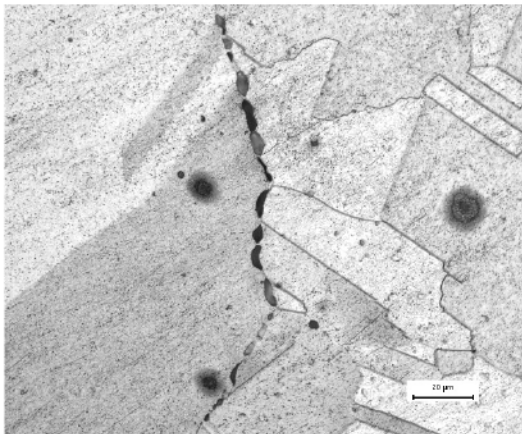
Figure 2-3. LOM images showing creep damage over the gauge length of creep testing samples. Material data is given in Table 2-2.



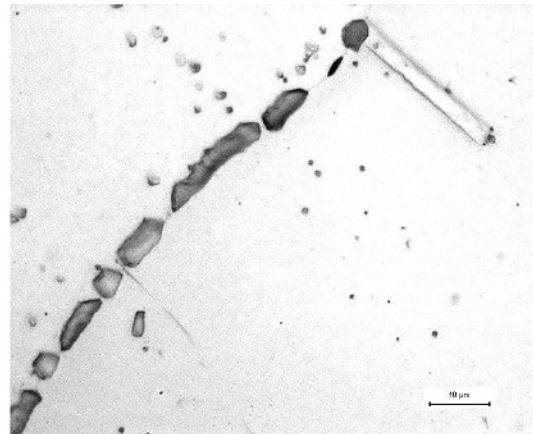
(a) Cu52, far away from fracture



(b) Cu15, a few mm away from fracture



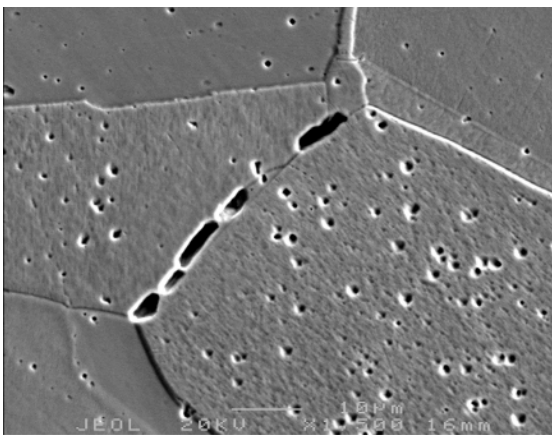
(c) Cu51, far away from fracture



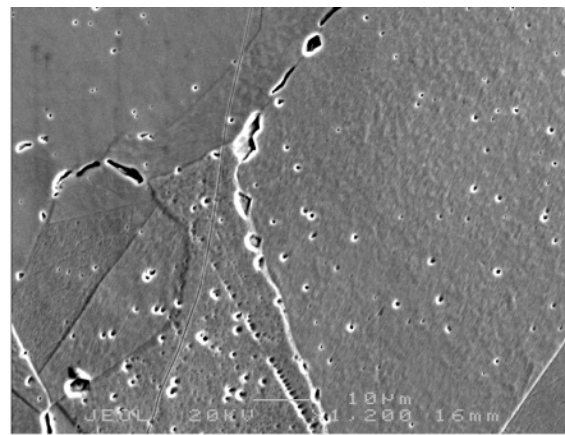
(d) Cu 101, adjacent fracture

Figure 2-4. LOM images showing intergranular creep cavitation and inclusions. Material data is given in Table 2-2.

The presence of intergranular creep cavities and cracks are verified by ASEM examinations, see Figure 2-5. Large cavities and cracks are frequently found in the ruptured specimens. There are many small voids inside the grains.



(a) Cu51



(b) Cu51

Figure 2-5. SEM images showing intergranular creep cavities and cracks. Material data is given in Table 2-2.

Attempts to identify the apparent grain boundary inclusions have been made on three samples, Cu51, Cu52, and Cu101 in both unetched and etched conditions in a SEM equipped with INCA analysis system. The results of chemical analyses of apparent grain boundary inclusions are given in Figure 2-6. Noting that the sample Cu52 in Figure 2-6b has been coated with gold in order to increase image quality. Surprisingly, only trace sulphur to a very low amount of 0.04 wt% is found on Cu51. On Cu52 and Cu101 there is no sulphur at all. The apparent inclusions in Figures 2-4 and 2-6 seem to be holes or cavities. The concentration of apparent sulphides is also very much higher than the total sulphur content would allow. In summary, it is very unlikely that the sulphides play an important role for the control of the creep ductility of copper.

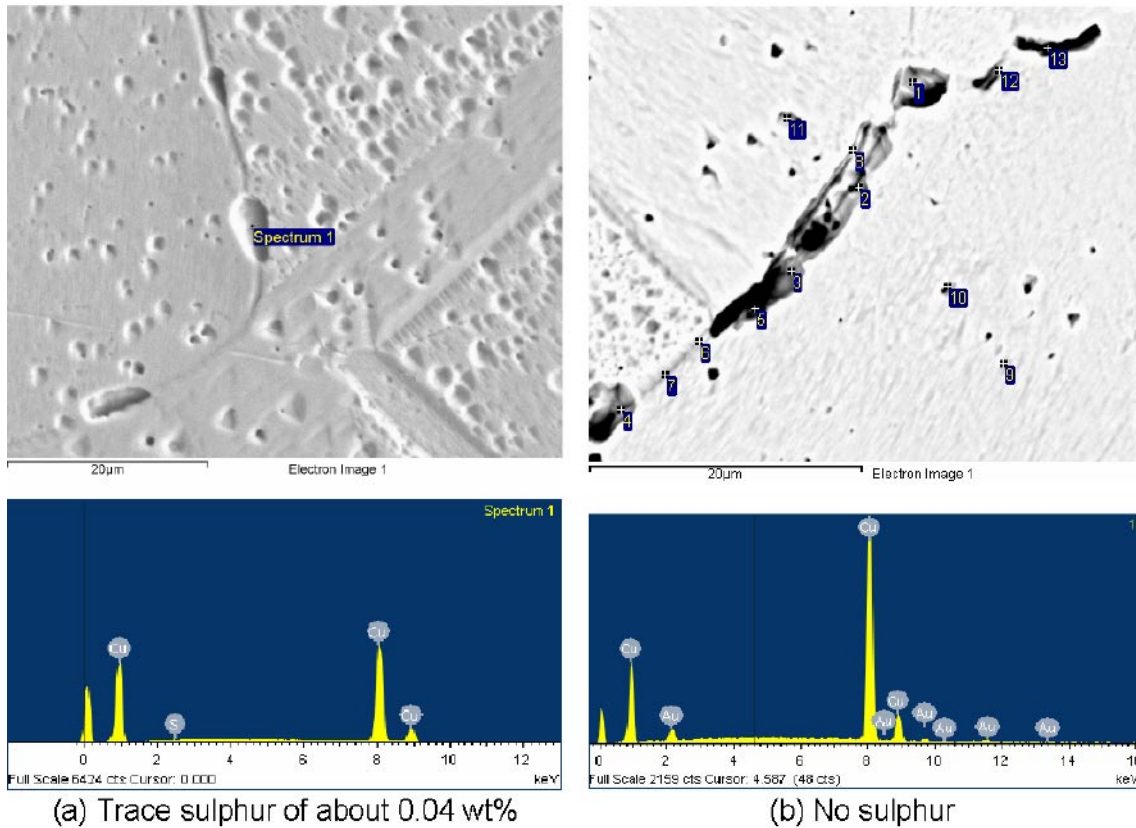


Figure 2-6. SEM images (upper) showing apparent grain boundary inclusions and spectrums (lower) showing elements detected for (a) sample Cu51 and (b) sample Cu52. Material data is given in Table 2-2.

3 Nucleation of creep cavities with the double ledge model

It is well known that creep cavities typically nucleate at grain boundaries. The nucleation takes place at particles, inclusions, as well as at ledges and other irregularities, see e.g. /8/. In the classical theory of nucleation, cavities are formed at the grain boundaries by clustering of vacancies. Raj gave the following expression for the nucleation rate $\frac{dn}{dt}$ /9/, /10/.

$$\frac{dn}{dt} = \frac{4\pi\gamma}{\sigma_n \Omega} \frac{\delta D_{BG}}{\Omega^{1/3}} N_{\max} \exp\left(-\frac{4\gamma^3 F_v}{\sigma_n^2 k_B T}\right) \quad (1)$$

where σ_n is the tensile stress driving nucleation perpendicular to the boundary, γ energy (per unit area) of the free surface, F_v a function which gives the volume of the critical cavity when multiplied by $r_c = 2\gamma/\sigma_n$ cubed, N_{\max} the maximum number of nucleation sites per unit area, Ω atomic volume, δD_{BG} boundary width multiplied by grain boundary self diffusion coefficient, k_B Boltzmann's constant and T the absolute temperature. In this thermal model random walk of vacancies leads to vacancy aggregations and eventually to stable cavities. Equation (1) gives a dramatic dependence of $\frac{dn}{dt}$ as a function of stress and temperature that is not observed during creep. Alternatively an athermal model can be considered where the local bounds are broken by the applied stress. However, Yoo and Trinkaus have demonstrated that during creep conditions the local stresses never exceed the grain boundary cohesive strength /11/. Thus, neither this athermal model can predict nucleation. One can conclude that the classical approaches are of limited value for modelling nucleation of creep cavities.

Experimentally it has been found that the number of cavities is approximately proportional to the creep strain. The nucleation rate can be expressed as

$$\frac{dn}{dt} = B\dot{\epsilon}_{cr} \quad (2)$$

where B is a constant and $\dot{\epsilon}_{cr}$ the creep rate. This relation was first observed for copper by Needham et al. /12/. Later, this behaviour has been seen many times for creep resistant steels, for a survey see Wu and Sandström /13/.

Next, a model will be presented that gives a relation of the form (2). It is assumed that the cavities are formed by grain boundary sliding. The sliding distance s_d is related to the creep strain /14/

$$s_d = C_s \dot{\epsilon}_{cr} \quad (3)$$

where C_s is a constant. The grain boundaries are assumed to have N_{inh} randomly distributed ledges or other inhomogeneities per unit area. A typical spacing l_{inh} between neighbour inhomogeneities is approximately

$$l_{inh} \approx \frac{1}{\sqrt{N_{inh}}} \quad (4)$$

The basic assumption in the model is that the grain boundaries consist of two closely spaced layers and that cavities are nucleated when an inhomogeneity on one layer meets one on the other layer. The model is referred to as the double ledge model. The number of encounters per unit area when two inhomogeneities meet is given by

$$n = \frac{s_d N_{inh}}{l_{inh}} \quad (5)$$

Combining Equations (3) to (5) gives

$$\frac{dn}{dt} = C_s N_{\text{inh}}^{3/2} \dot{\epsilon}_{\text{cr}} \quad (6)$$

Neither C_s nor N_{inh} is well known. As an order of magnitude estimate for copper at low temperatures, $C_s = 0.05 \mu\text{m}$ and $N_{\text{inh}}^0 = 1 \cdot 10^{14} \text{ 1/m}^2$ have been chosen, which gives $B = 5 \cdot 10^{13} \text{ 1/m}^2$. N_{inh}^0 is the constant part of N_{inh} , see below.

Due to the increasing diffusion around the grain boundaries with increasing temperature, one can expect that some of the inhomogeneities are gradually washed out. The smallest inhomogeneities that can prevail can be estimated with the help of Einstein's equation

$$l_{\text{inh min}} = \sqrt{\frac{2\delta D_{\text{GB}} t_{\text{diff}}}{d}} \quad (7)$$

where δD_{GB} is grain boundary diffusion coefficient, t_{diff} the typical diffusion time and d the grain diameter. The total number of inhomogeneities can now be expressed as

$$N_{\text{inh}} = \frac{1}{1/N_{\text{inh}}^0 + l_{\text{inh min}}^2} \quad (8)$$

Combining Equations (2) and (6)–(8) yields

$$B = \frac{C_s}{\left(1/N_{\text{inh}}^0 + 2\delta D_{\text{GB}} t_{\text{diff}} / d\right)^{3/2}} \quad (9)$$

Equation (2) was used by Danavas and Solomon in their modelling of creep cavitation in copper /15/. They determined the value of B by fitting to data from Raj at 750°C for a test with a rupture time of 328 h /16/. The grain size is given a large value 1,000 μm since bicrystals were used. Inserting these values gives $1.1 \cdot 10^6 \text{ 1/m}^2$. The value used in /15/ determined from the cavity data was $B = 1.6 \cdot 10^6 \text{ 1/m}^2$. This demonstrates that the diffusion term in Equation (9) can describe the temperature dependence of B approximately over a wide range of temperatures.

4 Growth of cavities

Two main types of processes contribute to the growth of creep cavities. In the first type the growth is controlled by diffusion. In the second type the growth is strain controlled. Many papers in the literature have derived expressions for the growth. An excellent review is given by Beere /17/. For the diffusion controlled growth the following equation has been used.

$$\frac{dR}{dt} = \frac{3\delta D_{GB}\Omega}{k_B T} \frac{\sin^2 \theta}{\theta - \sin \theta \cos \theta} \frac{L^2}{R(L-2R)^3} \left(\sigma - \frac{\gamma_s \sin \theta}{R} \right) \quad (10)$$

where R is the cavity radius in the grain boundary plane, Ω the atom volume, θ angle inside the cavity at the intersection with the grain boundary, L the cavity spacing, σ the applied stress, and γ_s the surface energy. Equation (10) has been applied to copper in /9/, /15/, and /17/.

The cavity spacing L is determined from the number of cavities per unit area n .

$$L = \frac{1}{\sqrt{n}} \quad (11)$$

To avoid that the cavities intersect on average, which is unphysical, Equation (2) for the nucleation is replaced by

$$\frac{dn}{dt} = B\dot{\epsilon}_{cr} \frac{L - 2R_{max}}{L} \quad (12)$$

where R_{max} is the radius of a cavity that has been formed at $t = 0$. When the intercavity distance is sufficiently large the dislocation creep of the matrix accelerates the cavity growth rates. This strain controlled growth can be expressed as /15/, /17/, and /18/

$$\frac{dR}{dt} = \frac{\sin^2 \theta}{\theta - \sin \theta \cos \theta} R\dot{\epsilon}_{cr} \quad (13)$$

The effects of the contributions from diffusion and strain controlled growth can be approximated by direct adding of Equations (10) and (13) /17/.

5 Creep deformation and rupture

The behaviour of the creep deformation of copper changes dramatically at lower temperatures. Below 175°C for Cu-OF and below 275°C for Cu-OFP creep is well inside the power law breakdown regime, i.e. the creep exponent is essentially larger than 5 to 8 /19/. A creep model that can handle this transition has recently been developed /19/. According to this model the creep rate can be expressed as

$$\dot{\epsilon}_{\text{OFP}} = \frac{2bc_L}{m} \frac{D_s b \tau_L}{k_B T} \left(\frac{\sigma}{\alpha G m b} \right)^3 e^{\frac{\sigma b^3}{k_B T}} e^{-\frac{Q_{\text{eff}}}{R_{\text{gas}} T} \left[1 - \left(\frac{\sigma}{\sigma_{\text{imax}}} \right)^2 \right]} / f_P \quad (14)$$

where b is Burgers vector, D_s is the volume self diffusion coefficient, τ_L is the dislocation line tension, c_L , m and α are constants, σ is the applied stress, R_{gas} is the gas constant, Q_{eff} is an activation energy and σ_{imax} is approximately the tensile strength. The values of the constants can be found in /19/. f_P is a function that takes into account the effect of phosphorus. f_P is equal to unity for Cu-OF and is for Cu-OFP given by

$$f_P = \frac{\dot{\epsilon}_{\text{OF}}}{\dot{\epsilon}_{\text{OFP}}} = \begin{cases} K_1 \exp(K_2 e^{-k_3 T}) & T > 348 \text{ K} \\ K_0 & T \leq 348 \text{ K} \end{cases} \quad (15)$$

K_0 , K_1 , K_2 , and k_3 are constants.

50 ppm phosphorus has a pronounced influence on the creep strength of copper. The cause of the effect is that the P atoms which are in solid solution form Cottrell atmospheres around the dislocations and lock them. A significant extra stress is needed to release the dislocations from the atmospheres /20/.

Both nucleation and growth of cavities are affected by the grain boundary sliding. If this process is slowed down both nucleation and the growth rate will be reduced. It is assumed that the interaction energy E between the solute and the grain boundary controls agglomeration of solutes ($E < 0$).

$$c_{\text{PGB}} = c_{\text{P0}} e^{-\frac{E}{k_B T}} \quad (16)$$

where c_{P0} is the average P-content in the copper and c_{PGB} is the concentration of P at the grain boundaries. To move the grain boundary an energy E per solute atom is needed. This energy is provided by the extra stress σ_{break} that is acting across the area b^2/c_{PGB} and the boundary moving one Burgers vector. This gives the energy balance

$$\sigma_{\text{break}} = \frac{2m}{b^3} E c_{\text{P0}} e^{-\frac{E}{k_B T}} \quad (17)$$

m is the Taylor factor that takes into account the transformation of a shear stress to a tensile stress. To take into account the locking of the grain boundaries, the applied stress in Equations (12) and (13) should be reduced by σ_{break} in Equation (17) when computing the nucleation and the growth rate for Cu-OFP.

Due to the cavitation a certain fraction A_{cav} of the grain boundaries areas will no longer be load carrying. The cavitated area fraction at time t can be expressed as

$$A_{\text{cav}} = \int_0^t \frac{dn}{dt'}(t') \pi R^2(t, t') dt' \quad (18)$$

$R(t,t')$ is the radius of the cavity at time t that was formed at time t' . If two approximations are made, Equation (18) can be simplified. The first one is that the intercavity distance L is significantly larger than the cavity size. According to Equation (12) the nucleation rate is then constant and can be placed outside the integral. The second approximation is that $R(t,t')$ depends only on $t-t'$ which is the case if L does not vary too much, see Equation (10). Taking the time derivative of Equation (18) then gives

$$\frac{dA_{\text{cav}}}{dt} = \frac{dn}{dt} \pi R^2(t) \quad (19)$$

Brittle creep rupture is assumed to take place when the cavitated area fraction has reached a value of $A_{\text{cav}} = 0.25$. The corresponding criterion for ductile rupture is that the creep strain is equal to 0.4. The criterion that is reached first controls the type of rupture.

6 Model predictions

6.1 Constants used in the computations

The values of constants that have been used in the computations are listed in Table 6-1.

6.2 Nucleation and cavity growth

Using Equations (2), (9), and (14) the number of cavities have been computed. The results are illustrated as a function of strain in Figure 6-1. As a starting value one cavity nucleus per grain has been assumed. The stresses have been selected to give rupture after 10,000 h.

The generation of new cavities starts at very small strains for Cu-OF. However, for Cu-OFP at 175°C 1% strain must be reached before significant new nucleation occurs. At 250°C the formation of cavities begin at small strains for both materials. At 250°C higher strains are needed for Cu-OFP to reach the same cavitation level as for Cu-OF. Once the initial situation is left the number of cavities is proportional to the strain.

Table 6-1. Values of constants in the computations

Parameter description	Parameter	Value	Ref.
Coefficient for self diffusion	D_{s0}	$1.31 \cdot 10^{-5} \text{ m}^2/\text{s}$	/21/
Activation energy for self diffusion	Q_s	198,000 J/mol	/21/
Coefficient for grain boundary diffusion	δD_{GB}^0	$6.49 \cdot 10^{-14} \text{ m}^2/\text{s}$	
Activation energy for grain boundary diffusion	Q_{GB}	119,000 J/mol	
Interaction energy for P^*		$2.49 \cdot 10^{-20} \text{ J}$	/19/
Burgers vector	b	$2.56 \cdot 10^{-10} \text{ m}$	
Strain hardening constant	c_L	57	
Taylor factor	m	3	
Boltzmann's constant	k_B	$1.381 \cdot 10^{-23} \text{ J/grad}$	
Constant in Equation (4)	α	0.19	
Shear modulus	G	$G = 4.75 \cdot 10^4 - 17T \text{ MPa}$, T in K	/22/
Activation energy for creep at high temperatures	Q_{eff}	198,000 J/mol	/22/
Max back stress	σ_{imax}	257 MPa	
Dislocation line tension	τ_L	$7.94 \cdot 10^{-16} \text{ MN}$	
No of inhomogeneties per unit area	N_{inh}^0	$1 \cdot 10^{14} \text{ 1/m}^2$	
Sliding rate constant	C_s	0.05 m	
Atom volume	Ω	$1.181 \cdot 10^{-29} \text{ m}^3$	
Cavity angle	θ	1.38 rad	
Surface energy	γ_s	1.73 J/m ²	/23/
Constants in Equation (15)	K_0, K_1, K_2, K_3	3,000, 0.1695, 55.73, 0.005 1/°C	
Grain size	d_{grain}	0.0001 m	

* Due to lack of data the value for dislocations has been applied.

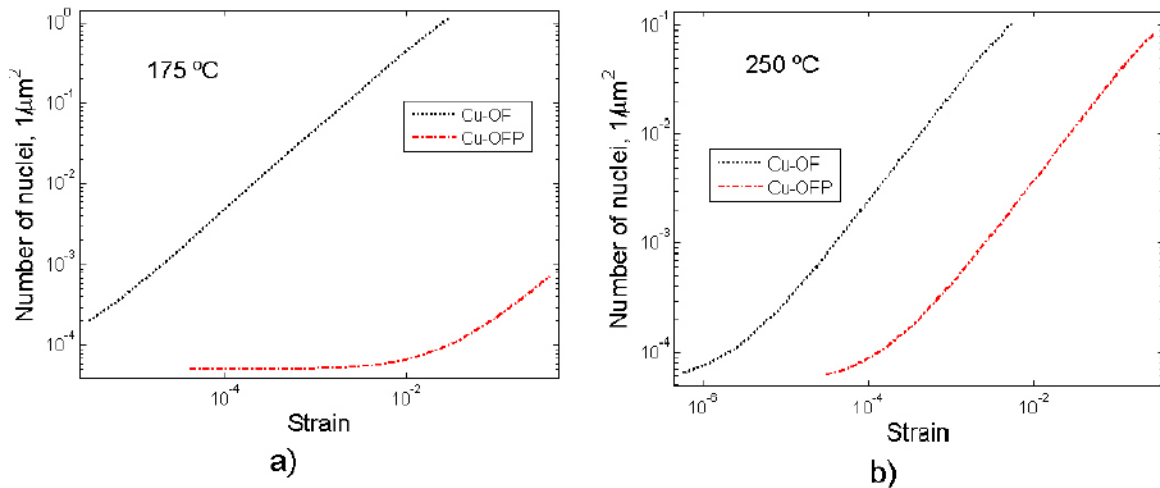


Figure 6-1. Number of cavities as a function of creep strain for Cu-OF and Cu-OFP at a) 175°C and b) 250°C. Based on Equation (2).

Using Equation (11) the cavity spacing can be determined from the number of cavities per unit area. The result is illustrated in Figure 6-2 as a function of time. It is interesting to note that the cavity spacing is almost the same for Cu-OF and Cu-OFP at 250°C for a given time but are very different at a given strain, see Figure 6-1.

The cavity spacing at 10,000 h as a function a temperature is illustrated in Figure 6-3. 10,000 h is the assumed rupture time. Cu-OF and Cu-OFP behave very differently. Cu-OF forms a large number of cavities already at low temperature, whereas no cavities appear below 150°C for Cu-OFP due to the efficient locking of the grain boundaries at low temperatures. Above 150°C the temperature dependence of the constant B (Equation 9) sets in and the cavity spacing of Cu-OF increases. Above 230°C the cavity spacing is quite similar for the two materials.

In Figure 6-2 the max cavity radius is shown as a function of time. The radius is computed using Equations (10) and (13) that are added. Usually the diffusion controlled contribution, Equation (10) is larger than the strain controlled contribution, Equation (13). It is the maximum cavity radius that is shown, i.e. a cavity that has nucleated at time zero. For Cu-OFP there is virtually no growth at 175°C whereas the growth for Cu-OF is significant. However, at 250°C the results are nearly the same for the two materials. In fact, the growth rate increases faster with

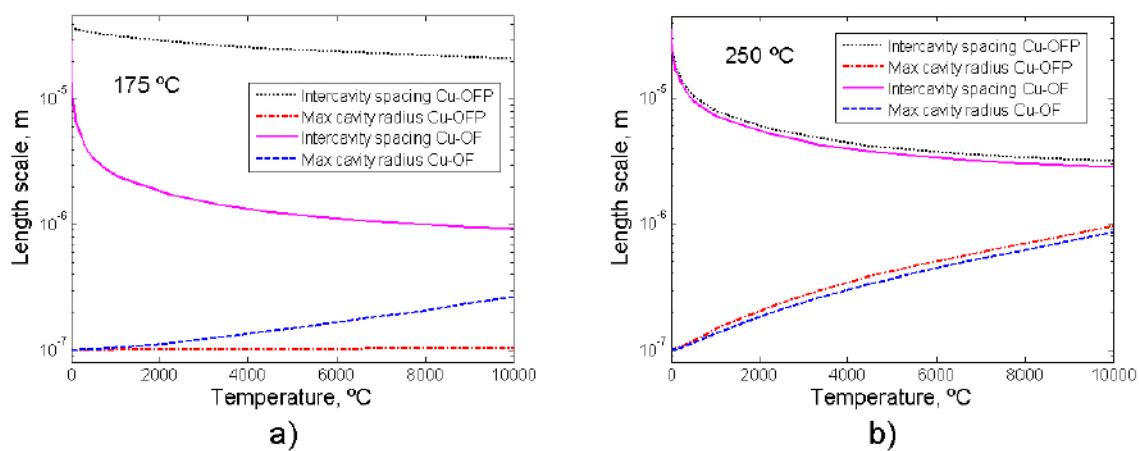


Figure 6-2. Cavity spacing and max cavity radius as a function of time for Cu-OF and Cu-OFP at a) 175°C and b) 250°C. Based on Equations (2), (10) and (12).

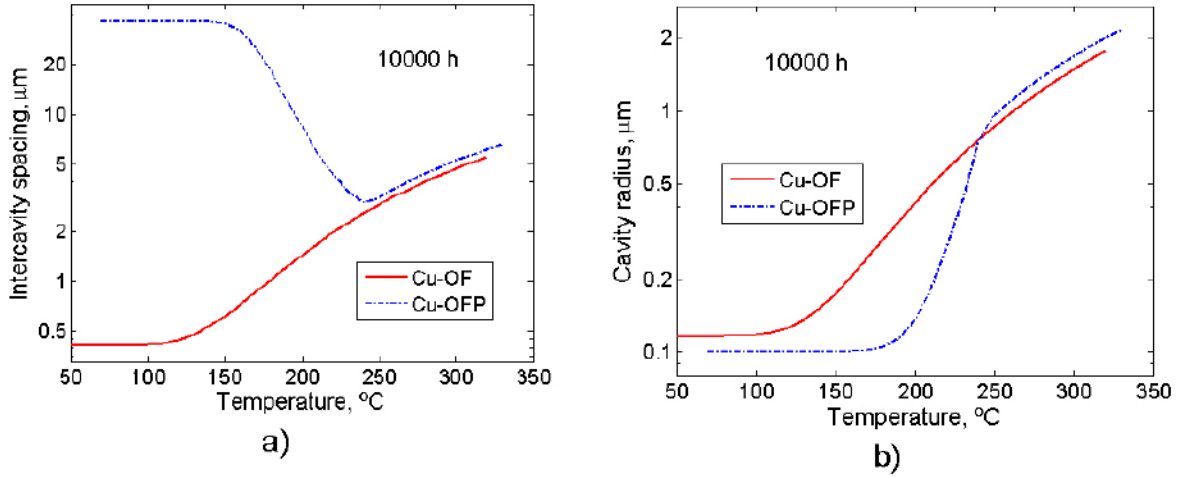


Figure 6-3. Cavity spacing (a) and cavity radius (b) at rupture (10,000 h) versus temperature.

temperature for Cu-OFP than for Cu-OF since the significance of the stress reduction term, Equation (17), is reduced with increasing temperature. This is shown in Figure 6-3b where the temperature dependence of the cavity radius at rupture is presented.

Results for the cavitated area fraction A_{cav} computed with the help of Equations (2), (10), (12) and (18) are shown in Figure 6-4.

A_{cav} increases approximately linearly with time for most of the time range in Figure 6-4. This is consistent with Equation (9). The rate of forming new cavities $\frac{dn}{dt}$ is fairly constant and the cavity R is approximately proportional to the square root of time, see Equation (10). At longer times R approaches $L/2$ and the cavity growth rate then increases, see again Equation (10). The temperature dependence of A_{cav} at rupture is illustrated in Figure 6-5.

For Cu-OF, $A_{cav} = 0.25$ is the rupture criterion over the whole temperature interval. This means that the cavitation consistently gives rise to brittle creep rupture. For Cu-OFP the rupture is ductile up to 240°C and the rupture is controlled by $\epsilon_R = 0.4$, where ϵ_R is the elongation at rupture. Above this temperature the rupture is brittle in the same way as for Cu-OF. The reason for this difference between the materials is that fewer cavities are formed and they grow slower in Cu-OFP than in Cu-OF below 240°C, see Figure 6-3.

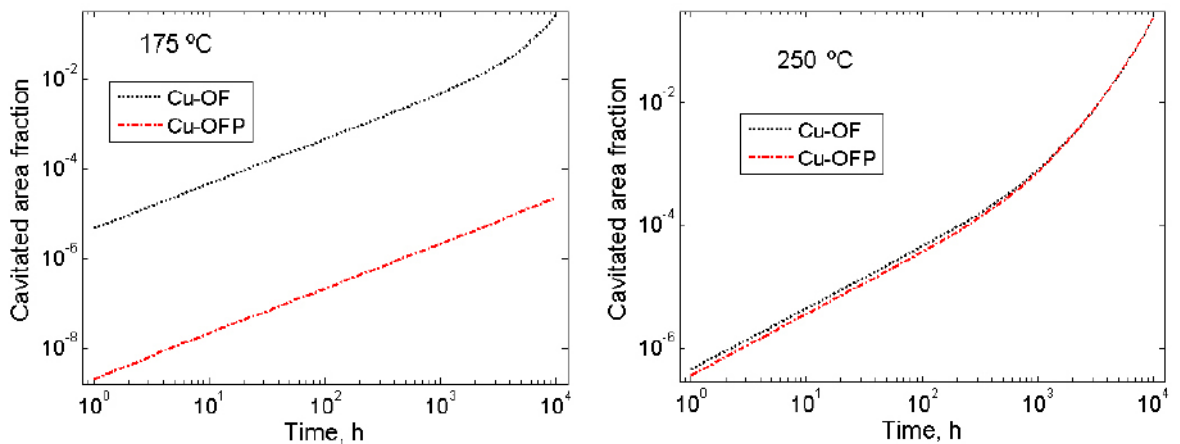


Figure 6-4. Cavitated area fraction as a function of time for Cu-OF and Cu-OFP at a) 175°C and b) 250°C. Based on Equations (2), (10), (12) and (18).

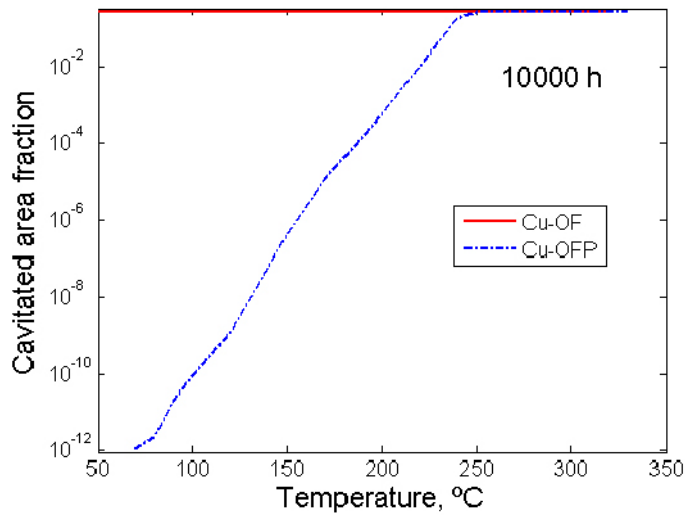


Figure 6-5. Cavitated area fraction at rupture versus temperature. Rupture time 10,000 h.

6.3 Ductility

As mentioned in section 5, rupture is assumed to take place when either of the criteria $A_{cav} = 0.25$ or $\epsilon_{cr} = 0.4$ is reached. To find the stress that gives rupture after a given time, Equations (14) and (18) are applied. These equations are solved by iteration. The chosen rupture time is 10,000 h. The resulting stresses are shown in Figure 6-6. Experimental data having a rupture time longer than 3,000 h are also shown. Above 200°C three points exist for Cu-OFP with rupture times around 3,000 h. They lie about a factor of 1.2 above the predicted line as they should. We can conclude that the rupture stress is predicted in a reasonable way.

The elongation values at rupture have been computed by means of Equation (14). The results are shown in Figure 6-7.

Both materials have a minimum in the creep ductility versus temperature. The minimum is much more pronounced for Cu-OF than for Cu-OFP. Furthermore, the minimum appears at lower temperatures for Cu-OF than for Cu-OFP. All this is fully consistent with the experimental data.

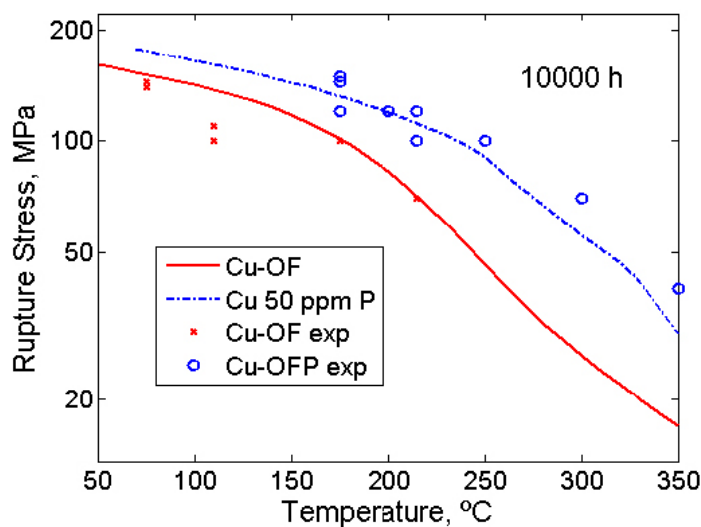


Figure 6-6. Stress that gives creep rupture after 10,000 h versus temperatures. The predictions are based on Equation (18) for $A_{cav} = 0.25$ or on Equation (14) for $\epsilon_{cr} = 0.4$. Experimental data with rupture times exceeding 3,000 h are shown. Model values for 50 ppm P.

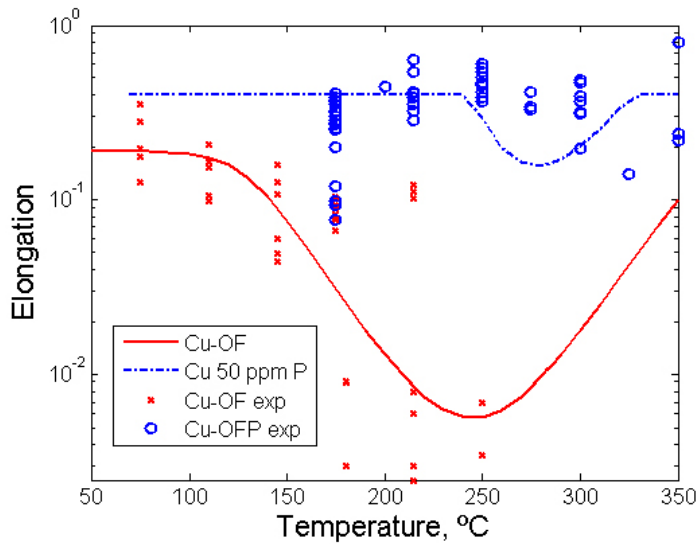


Figure 6-7. Creep elongation at rupture versus temperature calculated with Equation (14) for a rupture time of 10,000 h for Cu-OF and Cu-OFP. Measured creep elongation values are shown for comparison. Model values for 50 ppm P.

The minimum for Cu-OFP appears at slightly lower temperatures than in the observations. This demonstrates that the model to some extent underestimates the difference between the materials rather than overestimates it.

In SKB's specification the lowest content of phosphorus that is allowed is 30 ppm. It is therefore of interest to analyse how the rupture behaviour is affected. In Figure 6-8 the rupture stress is given as function of temperature for 30 ppm P.

If a comparison to Figure 6-6 is made, there is no change below 200°C for Cu-OFP. There is a slight reduction in strength above 200°C. The values for Cu-OF are of course not affected at all. For a P content of 80 ppm on the other hand the strength is further increased above 200°C, but the effect is quite small below this temperature. The values for the creep elongation at rupture for 30 ppm P is shown in Figure 6-8.

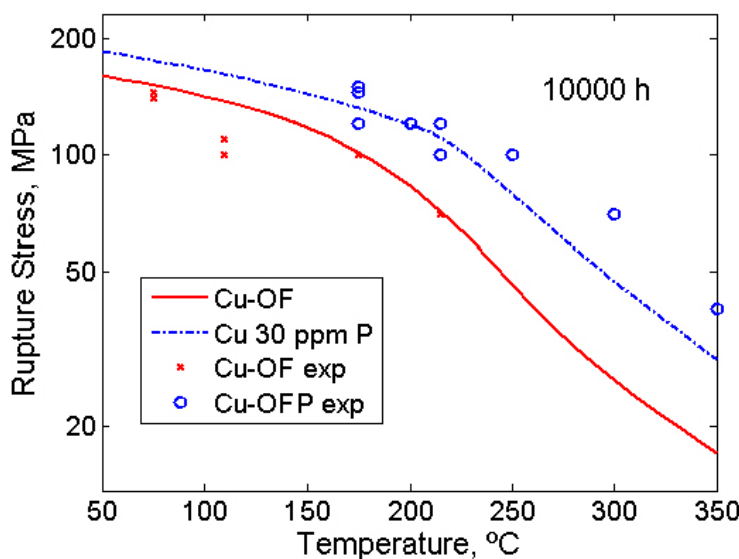


Figure 6-8. Same as Figure 6-6 with model values based on 30 ppm P.

The minimum in the elongation for Cu-OFP is more pronounced for 30 ppm P than for 50 ppm P and it is positioned at a slightly lower temperature, see Figure 6-7. The reduction in the ductility starts at around 210°C instead of at 230°C for 50 ppm P. If the P content is raised instead to 80 ppm the ductility minimum for Cu-OFP vanishes altogether.

All the computed results above use a rupture time of 10,000 h, i.e. a lifetime of a little more than one year. In Figure 6-10 it is illustrated how the creep elongation appears at a longer rupture time of 1,000,000 h (114 years). Because of the extended extrapolation, Figure 6-10 should only be considered to give general trends.

If Figures 6-9 and 6-10 are compared, it is evident that the ductility minimum for Cu-OF has about the same depth but is moved to lower temperatures at longer rupture times. For Cu-OFP on the other hand the depth of the ductility minimum is much reduced. It is also moved to lower temperatures but to a less extent than for Cu-OF. For even longer rupture times the ductility minimum disappears altogether for Cu-OFP.

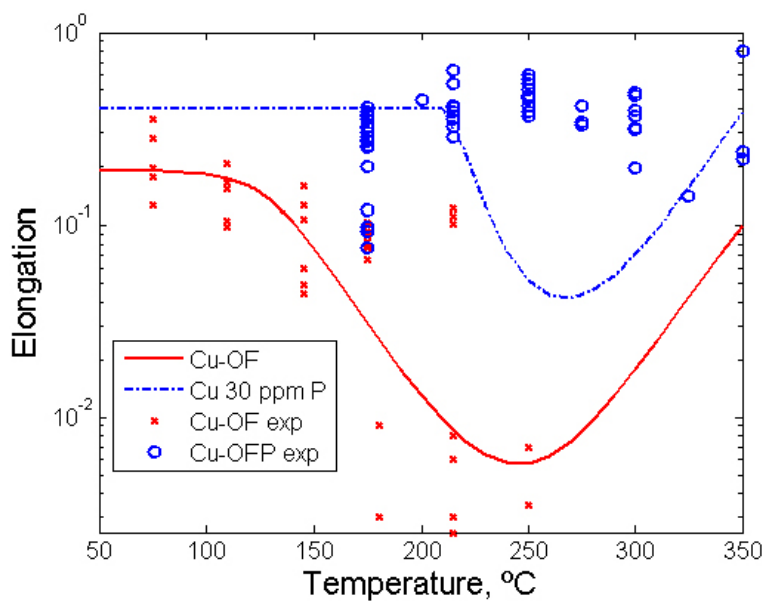


Figure 6-9. Same as Figure 6-7 with model values based on 30 ppm P.

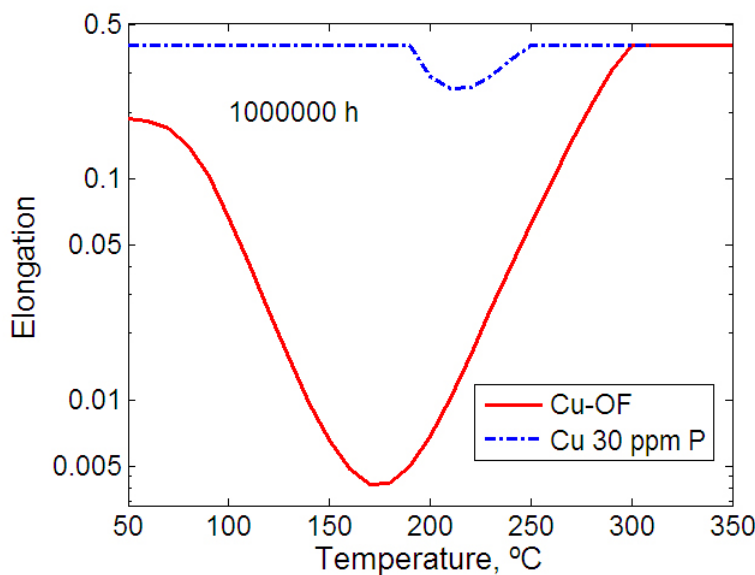


Figure 6-10. Creep elongation at rupture versus temperature calculated with Equation (14) for a rupture time of 1,000,000 h for Cu-OF and Cu-OFP. Model values with 30 ppm P.

7 Discussion

The cavity formation in previously performed creep tests of Cu-OF has been reassessed. In this material extra low creep ductility (ELCD) has been observed at temperatures above 175°C. In all performed tests the material has failed intergranularly. Creep cavities and cracks are observed to a varying extent on all samples, independent of creep ductility. These findings agree with the previous examinations.

Unexpectedly, the intergranular inclusions observed in previous studies are not seen in the present investigations, see Figures 2-4 and 2-6. The analysed inclusion-like objects were actually holes or cavities. In the light optical microscope, these objects are not as dark as other cavities and cracks, see again Figures 2-4 and 2-6. It is their light colour that may give rise to a misinterpretation, especially when they are located at grain boundaries. They look as if they are gray, possibly because they are shallow. SEM images illustrate that they are indeed holes or cavities, see Figure 2-6. INCA analyses further confirm that the objects do not contain any sulphur at all or only trace contents, see also Figure 2-6. With a bulk sulphur content of 10 ppm, very few sulphides can appear at the grain boundaries. In addition, creep cavitations are in many cases not associated with inclusions. Therefore, it can be concluded that it is unlikely that the main cause of ELCD is a reduction of the cohesive strength at the grain boundaries due to the formation of cavities around sulphides.

The formation and growth of cavities have been modelled ignoring the role of sulphur. For many materials including copper it has been observed that the rate of nucleation of cavities is proportional to the strain rate. The newly developed model for cavity formation shows this behaviour. It is natural to assume that the nucleation of cavities is controlled by grain boundary sliding. The amount of sliding is in turn proportional to the creep rate. The basic assumption in the model is that a cavity is formed when ledges on opposite sides of the grain boundary meet. For this reason the model is referred to as the double ledge model. The number of fine ledges decreases with increasing temperature due to diffusion, which implies that the rate of cavity formation is decreased. This effect is quite dramatic. As was demonstrated in the text, the nucleation rate was reduced by seven orders of magnitude when the temperature was raised from 150 to 750°C.

The growth of creep cavities has been extensively studied for many years and well established models are available. The growth can either be diffusion controlled or strain controlled. Both processes run in parallel and the model result from each of them can be added and that is what has been done in the present paper.

The influence of phosphorus on the creep deformation has been analysed in a previous paper /20/. This influence is due the creation of Cottrell atmospheres of P-atoms around the dislocations. For the dislocations to move they must break away from the Cottrell atmospheres and this requires an extra stress. In the same way the P-atoms agglomerate around the grain boundaries and create a substantial locking force. It has been shown that phosphorus can reduce the grain boundary mobility in copper /24/. The magnitude of the additional stress that is required to make the grain boundary slide has been derived. Since grain boundary sliding is essential for nucleation and growth of cavities, these processes are strongly affected by the presence of phosphorus.

Creep rupture can take place either in a ductile or a brittle mode. Brittle rupture happens when there is sufficient amount of cavitation on the grain boundaries. Thus, brittle rupture requires extensive nucleation and growth of cavities. If the formation and growth of cavities are slow, and the creep deformation is large before a significant fraction of the grain boundaries have cavitated, a creep specimen will fail by necking and a component by plastic instability in general. This criterion has been used in the present paper to predict the type of rupture. Cu-OF consistently shows brittle rupture in the investigated temperature interval. This is in full agreement with the predictions. Cu-OF on the other hand has an essentially ductile behaviour at lower temperatures with a limited number of creep cavities present. This is again in agreement with the modelling.

With the defined criteria the stresses that give rupture in a specified time can be determined. The predicted stresses agree with observed strengths for the investigated case with a rupture time of 10,000 h. In the same way the rupture ductility can be modelled. The calculated elongation reproduces the observed temperature dependence of the rupture ductility.

The influence of the phosphorus content on the creep ductility and the rupture strength has been computed. Most of the results that are presented in the paper refer to a phosphorus content of 50 ppm. For 30 ppm P the minimum in the ductility is wider and deeper than at 50 ppm, but the drop in the ductility is still above 200°C. If the P-content is raised to 80 ppm and above the ductility minimum disappears altogether.

At temperatures below 200°C the P-content has no influence on the rupture stress in the investigated interval 30 to 80 ppm. At the position of the ductility minimum around 260°C, however, the rupture strength increases somewhat with P-content. Experimentally the influence of the phosphorus content on the creep properties has mainly been studied at 175°C. Little or no effect on the creep strength and ductility was observed /4/. This is fully consistent to the model results since neither the strength nor the ductility is influenced when the P-content is changed from 30 to 80 ppm at this temperature.

The influence of the assumed rupture time on the creep elongation has been analysed briefly. For Cu-OF the ductility minimum moves to lower temperatures at longer rupture times essentially unchanged in magnitude. For Cu-OFP on the other hand the minimum is continuously reduced in size and eventually vanishes altogether at very long rupture time. Thus, the model predicts that there is no risk that the creep ductility minimum at high temperatures for short rupture times could be a safety issue at low temperatures even for the longest rupture times for Cu-OFP .

Previously it has been believed that sulphur embrittlement was the main cause of the extra low creep ductility in Cu-OF. With the results of the cavity model describing the temperature dependence of the ductility in an excellent way the cavitation is likely to be the main controlling factor.

8 Conclusions

1. The cavity formation in previously creep tested specimens of Cu-OF has been reassessed. Independent of material and ductility at rupture, cavitation to a varied extent and intercrystalline failure were found for all the examined samples.
2. Surprisingly, intergranular inclusions reported in the previous work are not found in the present investigations. SEM examinations reveal that apparent inclusions in fact can be holes or cavities. INCA analyses confirm that no sulphur or only trace sulphur is detected in these objects.
3. A new model has been derived for nucleation of cavities. In the model it is assumed that a cavity is formed when ledges on the opposite side of a grain boundary meet during grain boundary sliding. This model that is named the double ledge model, can explain why the rate of nucleation is proportional to the creep strain, a behaviour that has been observed for many creep resistant steels and for copper. Due to diffusion the efficiency of the ledges is reduced with increasing temperature. This can quantitatively explain why the nucleation rate is more than seven orders of magnitude higher per unit creep strain at 150 in comparison to at 750°C.
4. The cavity growth can be diffusion controlled or strain controlled. Models for the processes are well established. Both processes have been taken into account in the present work. In the temperature range studied diffusion control has been found to be dominating.
5. The cavitation in Cu-OF gives rise to creep brittle failure in all of the analysed tests in the temperature interval 75 to 250°C. The cavitation model predicts a deep minimum in the creep ductility of 0.5% around 250°C in excellent agreement with observations.
6. Phosphorus in Cu-OFP agglomerates at the grain boundaries and lock their sliding. The stress that is required to unlock the grain boundaries has been computed. This additional stress reduces the nucleation of cavities and to some extent also their growth. Based on these principles the cavitation model gives a much more shallow trough in the creep ductility for Cu-OFP than for Cu-OF and it is also moved to higher temperature. This is fully consistent with the experimental data.
7. A trough in the creep ductility that is smaller than for Cu-OF occurs at around 270°C for Cu-OFP. The model predicts that it is larger in size for 30 ppm P than for 50 ppm P and that it disappears altogether at 80 ppm P and above.
8. When the assumed rupture time is increased from 10,000 h (1.1 years) to 1,000,000 h (114 years) the magnitude of the creep ductility minimum is much reduced and vanishes for still longer rupture times for Cu-OFP according to the model. The temperature position of the minimum is only marginally affected by the rupture time. Thus, the model predicts that low creep ductility in the temperature range 0 to 100°C of technical interest for the canisters can be ruled out even for very long rupture times for Cu-OFP.

Acknowledgments

The authors would like to thank the Swedish Nuclear Fuel and Waste Management Co for funding this work.

References

- /1/ **Werme L, 1998.** Design premises for canister for spent nuclear fuel. SKB TR-98-08, Svensk Kärnbränslehantering AB.
- /2/ **Henderson P, Österberg J-O, Ivarsson B, 1992.** Low temperature creep of copper intended for nuclear waste containers. SKB TR-92-04, Svensk Kärnbränslehantering AB.
- /3/ **Henderson P, Sandström R, 1998.** Low temperature creep ductility of OFHC copper, Mat. Sci. Eng., A246, pp 143–150.
- /4/ **Andersson H, Seitisleam F, Sandström R, 1999.** Influence of phosphorous and sulphur as well as grain size on in creep pure copper. SKB TR-99-39, Svensk Kärnbränslehantering AB.
- /5/ **Lindblom J, Henderson P, Seitisleam F, 1995.** Creep testing of oxygen-free phosphorus copper and extrapolation of the results, Corrosion and Metals Research Institute, IM-3197.
- /6/ **Korzhavyi PA, Abrikosov I A, Johansson B, 1999.** Theoretical investigation of sulfur solubility in pure copper and dilute copper-based alloys, Acta mater. Vol. 47, No. 5, pp 1417–1424.
- /7/ **Ivarsson B, Österberg J-O, 1988.** Creep properties of welded joints in OFHC copper for nuclear waste containment. SKB TR-88-20, Svensk Kärnbränslehantering AB.
- /8/ **Evans RW, Wilshire B, 1993.** Introduction to Creep, The Institute of Materials, London, UK.
- /9/ **Raj R, 1978.** Nucleation of cavities at second phase particles in grain boundaries, Acta metall. 26, pp 995–1006.
- /10/ **Raj R, Ashby M F, 1975.** Intergranular fracture at elevated temperature, Acta metall. 23, pp 653–666.
- /11/ **Yoo M H, Trinkaus H, 1983.** Crack and Cavity Nucleation at Interfaces During Creep, Metall. Trans A. Vol. 14A, No. 4, pp 547–561.
- /12/ **Needham N G, Wheatley J E, Greenwood G W, 1975.** The creep fracture of copper and magnesium, Acta Metallurgica Vol. 23, pp 23–27.
- /13/ **Wu R, Sandström R, 1996.** Strain dependence of creep cavity nucleation in low alloy and 12% Cr steels, Mater. Science Techn. 12, pp 405–415.
- /14/ **Gifkins R C, 1994.** Grain-boundary participation in high-temperature deformation: an historical review, Materials Characterization 32, pp 59–77.
- /15/ **Davanas K, Solomon A A, 1990.** Theory of intergranular creep cavity nucleation, growth and interaction, Acta metall, mater. Vol. 38, No. 10, pp 1905–1916.
- /16/ **Raj R, 1978.** Intergranular fracture in bicrystals, Acta metall. 26, pp 341–349.
- /17/ **Beere W, 1981.** Cavities and Cracks in Creep and Fatigue (edited by J. Gittus). Applied Science, New York.
- /18/ **Chuang T-J, Kagawa K I, Rice J R, Sills L B, 1979.** Non-equilibrium models for diffusive cavitation of grain interfaces, Acta metall. 27, pp 265–284.
- /19/ **Sandström R, Andersson H C M, 2007.** Creep in Cu-OFP during power-law breakdown, Accepted for publ. in J Nuclear Materials.

- /20/ **Sandström R, Andersson H C M, 2007.** Influence of phosphorus on creep of copper, Accepted for publ. in J Nuclear Materials.
- /21/ **Neumann G, Tölle V, Tuijn C, 1999.** Monovacancies and divacancies in copper: Reanalysis of experimental data, Physica B: Condensed Matter, Volume 271, Issues 1–4, November (1999), pp 21–27.
- /22/ **Raj SV, Langdon T G, 1989.** Creep behaviour of copper at intermediate temperatures-I. Mechanical characteristics, Acta Metall. 37, 843.
- /23/ **Hirth J P, Lothe J, 1968.** Theory of Dislocations, McGraw-Hill, New York.
- /24/ **Hutchinson W B, Ray R K, 1979.** Influence of phosphorus on annealing behaviour of cold-worked copper, Metal Science 13, pp 125–130.

ISSN 1404-0344

CM Digitaltryck AB, Bromma, 2007